JGR Earth Surface

RESEARCH ARTICLE

10.1029/2020JF006040

Key Points:

- We simulate the Northern Hemisphere Ice Sheets over the last glacial cycle with a coupled ice sheet-glacial isostatic adjustment model
- We separate the influences of solid Earth deformation and gravitational field perturbations on Northern Hemisphere ice sheet dynamics
- Solid Earth deformation enhances ice volume changes and gravitational field perturbation stabilizes marine-based ice sheets

Supporting Information:

Supporting Information may be found in the online version of this article.

Correspondence to:

H. K. Han,
holly.han@mail.mcgill.ca

Citation:

Han, H. K., Gomez, N., Pollard, D., & DeConto, R. (2021). Modeling Northern Hemispheric ice sheet dynamics, sea level change, and solid Earth deformation through the last glacial cycle. *Journal of Geophysical Research: Earth Surface*, *126*, e2020JF006040. https://doi.org/10.1029/2020JF006040

Received 13 DEC 2020
Accepted 25 FEB 2021

Modeling Northern Hemispheric Ice Sheet Dynamics, Sea Level Change, and Solid Earth Deformation Through the Last Glacial Cycle

Holly Kyeore Han[1], Natalya Gomez[1], David Pollard[2], and Robert DeConto[3]

[1]Earth and Planetary Sciences Department, McGill University, Montreal, QC, Canada, [2]Earth and Environmental Systems Institute, Pennsylvania State University, University Park, PA, USA, [3]Department of Geosciences, University of Massachusetts, Amherst, MA, USA

Abstract Retreat or advance of an ice sheet perturbs the Earth's solid surface, rotational vector, and the gravitational field, which in turn feeds back onto the evolution of the ice sheet over a range of timescales. Throughout the last glacial cycle, ice sheets over the Northern Hemisphere have gone through multiple growth and retreat phases, but the dynamics during these phases are not well understood. In this study, we apply a coupled ice sheet-glacial isostatic adjustment model to simulate the Northern Hemisphere Ice Sheets over the last glacial cycle. We focus on understanding the influence of solid Earth deformation and gravitational field perturbations associated with surface (ice and water) loading changes on the dynamics of terrestrial and marine-based ice sheets during different phases of the glacial cycle. Our results show that solid Earth deformation enhances glaciation during growth phases and melting during retreat phases in terrestrial regions through ice-elevation feedback, and gravitational field perturbations have a stabilizing influence on marine-based ice sheets in regions such as Hudson Bay in North America and Barents and Kara Seas in Eurasia during retreat phases through sea-level feedback. Our results also indicate that solid Earth deformation influences the relative sensitivity of the North American and Eurasian ice sheets to climate and thus the timing and magnitude of their fluctuations throughout the last glacial cycle.

1. Introduction

During the last glacial cycle, ice sheets in the Northern Hemisphere (Northern Hemispheric Ice Sheets, henceforth NHIS) went through multiple phases of growth and retreat during the buildup phase (~120-21 ka; e.g., Dyke, 2004; Hughes et al., 2016; Kleman et al., 2010; Svendsen et al., 2004) until global ice volume and extent reached a maximum and global mean sea level was ~130 m lower than at present day at the Last Glacial Maximum (~26.5-21 ka; LGM; Austermann et al., 2013; Clark et al., 2009; Denton & Hughes, 1981). At the LGM, the British-Irish, Fennoscandian, and Barents-Kara Ice Sheets (BKIS) covered Eurasia (Eurasian Ice Sheet Complex, henceforth EISC; Hughes et al., 2016), the Laurentide, Cordilleran and Innuitian Ice Sheets covered North America (North American Ice Sheet Complex, henceforth NAISC; Dyke, 2004), and the Greenland Ice Sheet (GIS) grew beyond its modern extent (Fleming & Lambeck, 2004). After the LGM, the EISC and NAISC retreated throughout the last deglaciation, ending in the final retreat of the Fennoscandian Ice Sheet by ~9 ka (e.g., Cuzzone et al., 2016; Hughes et al., 2016) and the Laurentide Ice Sheet (LIS) by ~7 ka (Ullman et al., 2016). The last deglaciation phase ended with subsequent slowing of melting from the Antarctic and GIS by ~4 ka (Yokoyama et al., 2019).

Understanding the glacial-cycle dynamics of the NHIS is challenging since the ice sheet evolution is coupled with other components of the Earth system, and direct records of the long-term ice sheet evolution are limited because they are eroded away over multiple growth and retreat phases (Dyke et al., 2002; Kleman et al., 2010). A broad spectrum of modeling work has been done to explore the dynamics of the NHIS throughout the last glacial cycle, even when focusing only on the literature that studies the Northern Hemisphere as a whole (e.g., Abe-Ouchi et al., 2013; Banderas et al., 2018; Berends et al., 2018; Bonelli et al., 2009; Charbit et al., 2007; Ganopolski et al., 2010; Liakka et al., 2016; Niu et al., 2019; Tarasov & Peltier 1997; Zweck & Huybrechts, 2005), during the pre-LGM buildup phase (Beghin et al., 2014; Charbit et al., 2013; Kleman et al., 2013; Stokes et al., 2012; Timmermann et al., 2010) and during the last deglaciation phase

(Gregoire et al., 2015; Tarasov et al., 2012; Ullman et al., 2015). These studies have focused on different physical processes such as ice-atmosphere interactions (Beghin et al., 2014; Liakka et al., 2016), ice-ocean interactions (Timmermann et al., 2010), the role of orbital and greenhouse gas forcing on the evolution of the NHIS (Abe-Ouchi et al., 2013; Bonelli et al., 2009; Ganopolski et al., 2010; Gregoire et al., 2015), ice-sheet sensitivity to climate forcing (Banderas et al., 2018; Berends et al., 2018; Charbit et al., 2007; Tarasov & Peltier, 1997), ice-sheet sensitivity to climatological or glaciological model parameters (Charbit et al., 2013; Zweck & Huybrechts, 2005), and ice-sheet sensitivity to isostatic solid Earth deformation (Crucifix et al., 2001; van den Berg et al., 2008).

It has long been recognized that mass exchange between ice and water on the solid surface perturbs the gravitational field and rotation vectors and deforms the solid Earth. These responses together—termed "Glacial Isostatic Adjustment" (GIA)—lead to spatially and temporally variable changes in the elevations of the solid surface and the sea surface (e.g., Farrell & Clark, 1976; Mitrovica & Milne, 2002). The effects of GIA, in turn, feed back onto the dynamics and mass balance of ice sheets. In the interior of an ice sheet, viscoelastic deformation of the solid Earth underneath the ice alters the ice surface elevation, changing atmospheric conditions (i.e., temperature and precipitation) and feeding back onto the surface mass balance of the ice sheet (termed the "ice-elevation feedback"; e.g., Levermann & Winkelmann, 2016). For example, when an ice sheet melts and the ice surface elevation is lowered, increases in air temperature (lapse rate-induced) and precipitation (due to warmer air) lead to increased surface melting and accumulation, feeding back either negatively or positively onto the ice sheet's surface mass balance. On the edge of an ice sheet, solid Earth depression and associated changes in ice surface slopes enhance ice flux into the ablation zone (Schoof, 2007; Weertman, 1974). If an ice sheet is marine-based and terminates in water, changes in local water depth due to changes in the solid Earth surface and gravitational equipotential surface feed back onto the ice mass flux across the grounding line (the so-called sea-level feedback; e.g., Gomez et al., 2010). When a marine-based ice sheet loses mass, the solid Earth is uplifted and the sea surface height drops near the retreating ice sheet because of the weakened gravitational attraction between ice and ocean (henceforth "ice-ocean gravity"), leading to a local sea level fall that acts to stabilize the ice sheet (Gomez et al., 2010).

Despite this existing knowledge of feedbacks between ice sheet dynamics, sea level change and solid Earth deformation, it is only recently that modeling studies have developed fully coupled, dynamic ice sheet-GIA models. Coupled models have been applied to simulate the evolution of the past and future Antarctic Ice Sheet (Gomez et al., 2013, 2015, 2018; Konrad et al., 2015) and past global ice sheets (de Boer et al., 2014), but are not yet applied extensively to the Northern Hemisphere. Unlike the Antarctic Ice Sheet where temperatures are colder, surface melting is minimal and ice mass loss happens dominantly through dynamic flow of ice across the grounding line (e.g., Shepherd et al., 2018), the dynamics of the NHIS are strongly sensitive to atmospheric forcing (e.g., Bonelli et al., 2009; Charbit et al., 2007; Niu et al., 2019) and hence the ice-elevation feedback would have played a significant role in NHIS evolution during the last glacial cycle. At the same time, the sea-level feedback would have influenced the dynamics of marine-based sectors of ice sheets in regions such as Barents and Kara Seas in Europe and over Hudson Bay in North America.

While paleo-ice sheet and sea level observations are extensive in the Northern Hemisphere, the processes driving observed changes remain often poorly understood. For example, the ice sheet mechanisms associated with meltwater pulse events (observed in relative sea level records; Fairbanks, 1989; Harrison et al., 2019) and Heinrich events (observed in ice-rafted debris records; Heinrich, 1988) are still debated. Furthermore, uncertainty remains in the individual contributions from the NAISC, EISC, and GIS to observed sea level changes (e.g., Bassis et al., 2017; MacAyeal, 1993). In addition, a number of recent studies (Batchelor et al., 2019; Carlson et al., 2018; Dalton et al., 2019; Pico et al., 2017) have proposed that the LIS was smaller than previously thought during the Marine Isotope Stage 3 (Lisiecki & Raymo, 2005) and rapidly grew up to its LGM extent, but the processes driving this potential change remain relatively unexplored. In this regard, applying a coupled ice sheet-GIA model to the NHIS can both provide insight into the driving mechanisms of ice sheet change, and facilitate modeling glaciologically consistent paleo-ice sheet evolution synchronously with associated gravitationally consistent, spatially variable sea-level change, which can be directly compared to geomorphological data of ice-sheet change (e.g., terminal moraines, proglacial deposits, or esker) and geophysical data of sea-level change (e.g., local relative sea-level records, GRACE data or present day GPS uplift rates).

In this study, we couple a dynamic ice sheet model with a global GIA model and apply the coupled model to simulate the NHIS over the last glacial cycle. Our central goal is to understand the influence of solid Earth deformation and spatially variable gravitational field (and thus sea surface height) changes associated with surface (ice and ocean) loading redistribution on the evolution of the NHIS during growth and retreat phases throughout the last glacial cycle, which we term "deformational effects" and "gravitational effects," respectively. In the following sections, we introduce the ice sheet and GIA models and the coupling procedure (Section 2), show the results of NHIS ice volume changes over the last glacial cycle from simulations that include deformational and gravitational effects both separately and together, and explore how each effect plays a role in the distribution and timing of ice cover changes in North America and Eurasia during growth and retreat phases (Section 3). We finish with a discussion of our results in the context of existing literature (Section 4) followed by conclusions (Section 5).

2. Methods

2.1. Coupled Ice Sheet—Glacial Isostatic Adjustment Modeling

We couple a dynamic ice sheet model to a GIA model using the coupling algorithm described by Gomez et al. (2013) that has been previously applied to the past and future evolution of the Antarctic Ice Sheet. We review the key aspects of the modeling here, and more detailed descriptions of each model and the coupling procedure can be found in the following studies: Pollard and DeConto (2009, 2012)—ice sheet model, Gomez et al. (2013, 2015)—GIA model and coupling methods. The ice sheet model (Pollard & DeConto, 2012) combines shallow ice approximation and shallow shelf approximation (SSA) dynamics. The ice flux across the grounding line is parameterized following Schoof (2007), which avoids the need for high resolution around the grounding zone and allows long-term and large-scale simulations to be feasible. The simplified dynamics capture grounding-line migration reasonably well in idealized intercomparisons (Pattyn et al., 2012, 2013), although with somewhat larger differences on smaller space and timescales (Drouet et al., 2013; Pattyn & Durand, 2013). The spatial resolution of the ice sheet model is 0.5-degree latitude and 1-degree longitude on a regular lat-lon grid, on which the domain of the model spans 35°N-90°N in latitude and 0–360 degrees in longitude. The time resolution for the ice model is 0.5 year.

Climate forcing is obtained from a matrix of general circulation model (GCM) solutions for prescribed orbital configurations, atmospheric CO_2 levels and ice sheet sizes (DeConto & Pollard, 2003; Pollard, 2010; Pollard & DeConto, 2005). The GCM is the Global Environmental and Ecological Simulation of Interactive Systems (GENESIS) version 3 (Thompson & Pollard, 1997) and is run in spectral resolution of T31 (i.e., 48 latitude by 96 longitude cells). Each GCM solution contains an equilibrated climate condition for given prescriptions of the aforementioned variables. At any point during an ice sheet model simulation, monthly air temperature and precipitation are obtained by interpolating the values between the GCM-solution matrix. Monthly air temperature and precipitation are then interpolated in time to 5-day-time-step (which is the time-stepping of our surface mass balance model) annual cycle, after which the annual climate is bilinearly interpolated from the GCM grid to the ice model grid. In this procedure, a lapse rate correction from the topography assumed in the GCM matrix solutions to the modeled ice surface elevation is applied to both temperature and precipitation. While the appropriate lapse-rate value is uncertain, we use an atmospheric lapse rate of 8°C/km, which is larger than what is suggested in some studies (e.g., Abe-Ouchi et al., 2007) but within the range used in other previous studies (e.g., Erokhina et al., 2017; Marshall et al., 2002). In the supporting information, we show equations for the lapse rate correction and the sensitivity of the NHIS volume to different parameter values used in the correction (Figure S4). In calculating surface mass balance, we consider explicit snow and embedded liquid amount in pore space and allow refreezing and runoff of meltwater, where runoff only happens when snowpack is saturated with embedded liquid. Surface melt is computed by solving a linearized surface energy flux equation instead of using the Positive-Degree-Day scheme. We use a sub-grid scheme that straightforwardly interpolates the sloping ice surfaces within each cell and performs separate surface mass balance calculations for sub-grid portions of the cell before averaging them together, which reduces the dependency of the calculations on the model resolution. In the matrix climate forcing, GCM sensitivities are adjusted by multiplying the climate differences (temperature and precipitation) between pairs of matrix solutions by 2.5 due to orbital changes (the orbital forcing is shown in Figure S1), and by 1.05 due to ice-sheet-extent changes. These ad hoc adjustments represent uncertainty in the GCM climate sensitivities and are needed to achieve reasonably realistic orbital scale and 100-ky ice sheet cycles in our current ice sheet model. We note that the focus of this study is on the sensitivity of ice sheet variations to ice-Earth-sea level feedbacks (rather than comparing our model results to data-based ice sheet reconstructions), and the climate is adjusted simply to yield overall realistic cycles, that is, with repeated growth and retreat phases on orbital time scales expanding toward a maximum similar to the LGM, followed by a relatively rapid and complete or near-complete deglaciation similar to that since the LGM. In future work, we plan to improve the climate modeling.

For basal sliding, we use the Weertman sliding law with an exponent $m = 2$ (Weertman, 1957). The basal sliding coefficient is set to high (i.e., deformable sediment and faster ice flow) 10^{-6} m a^{-1} Pa^{-2} in regions in which the present-day topography is ocean-covered, and low (i.e., hard rock and slower ice flow) at 10^{-7} m a^{-1} Pa^{-2} in regions in which the present-day topography is above the sea level. In the supporting information, we perform additional simulations with more complex basal sliding coefficients based on the sediment distribution suggested by Gowan et al. (2019) and show that our conclusions remain the same.

The GIA model solves the general sea level theory described by Mitrovica and Milne (2003), Kendall et al. (2005), and Gomez et al. (2010). The model considers ice cover changes and a radially varying viscoelastic Earth structure as inputs and computes the responses of the solid Earth and gravitational field associated with changes in surface (ice and ocean) loading. We assume a spherically symmetric, self-gravitating viscoelastic Earth model (so-called SGVE; Peltier, 1974) that is rotating (Mitrovica et al., 2001), and adopt the elastic and density profile of the Earth structure from the seismic model PREM (Dziewonski & Anderson, 1981). Unless otherwise indicated, we adopt a lithospheric thickness of 120 km and upper and lower mantle viscosity of 5×10^{20} and 5×10^{21} PaS, respectively. The GIA model performs simulations with a resolution of spherical harmonic degree and order 512, and the solutions account for the multi-normal response of the viscoelastic Earth to surface loading (Peltier, 1974). Since the dynamic ice sheet model simulates ice cover changes only over the Northern Hemisphere, we adopt the Antarctic Ice Sheet history from the ICE-6G_C model (Argus et al., 2014; Peltier et al., 2015) to produce global ice coverage as an input to the GIA model.

The coupling procedure is as described by Gomez et al. (2013). Initial conditions for coupled ice sheet-GIA model simulations are taken from a previous ice sheet model simulation that is spun up to reach an equilibrium initial state at the last interglacial (125 ka) where only the GIS exists in the Northern Hemisphere. Initial topography in the ice sheet model domain (35°N-90°N latitude) is given by the ETOPO2 modern global topography data set (National Geophysical Data Center, 2006). The initialized ice configuration and topography in the Northern Hemisphere are then passed to the GIA model, and merged with ICE-6G_C ice history and topography outside the ice sheet model domain (90 S-35 N latitude). The initial topography for this domain (90 S-35 N latitude) is computed from a standalone GIA model simulation with ICE-6G_C over the last glacial cycle in which the predicted modern topography converges with the ETOPO2 topography.

At the start of a coupled simulation, the dynamic ice sheet model computes ice sheet change over the Northern Hemisphere every 0.5 years for the duration of a coupling interval (200 years) and passes the thickness of the ice sheets at the end of the coupling interval to the GIA model. The GIA model then merges the ice cover predicted by the ice sheet model in the Northern Hemisphere and ICE6G_C ice history in Antarctica and computes global variations in sea level due to ice loading changes across the current coupling interval. The resulting sea level change is passed back to update the bedrock elevation and the sea level in the ice sheet model, and the ice sheet model runs forward for the next coupling interval. This process continues throughout the coupled simulation.

In order to consider the effects of solid Earth deformation and spatially varying gravitational-field changes on the evolution of the NHIS throughout the last glacial cycle (i.e., deformational and gravitational effects), we perform four different coupled ice sheet-GIA model simulations in the main text: 1) a simulation on a viscoelastic, rotating Earth in which the GIA model accounts for spatially varying gravitational field changes due to ice-ocean gravity (referred to as a "fully coupled" simulation), 2) a simulation on a viscoelastic rotating Earth in which ice-ocean gravity is not incorporated and the sea surface height shifts uniformly across the globe (referred to as a "deformable Earth-noIOG" simulation; as done by Gomez et al., 2013), and 3) a simulation on a rigid, rotating Earth in which ice-ocean gravity is accounted for (referred to as a "rigid

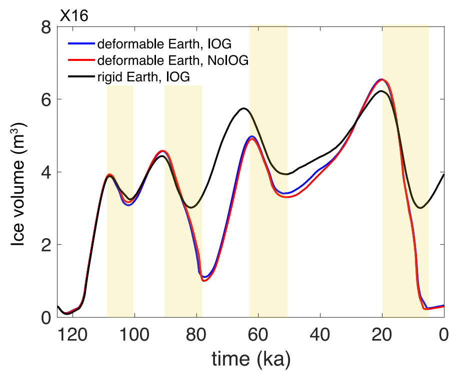

Figure 1. Changes in the Northern Hemisphere ice volume over the last glacial cycle. Time series of total Northern Hemisphere ice volume simulated with a coupled ice sheet-GIA model on a deformable Earth that captures the full multi-normal mode response (blue line), on a rigid Earth (black line), and for a simulation on a deformable Earth that neglects ice-ocean gravity (red line).

Earth-IOG" simulation). In the supporting information, we review the modified sea level equation for these coupled simulations excluding ice-ocean gravity and solid Earth deformation. We note that we have varied our model setup by repeating these simulations at a range of ice sheet model resolutions adopting a range of model parameters (i.e., basal sliding coefficients, surface mass balance and Earth structure parameters) controlling the distribution of ice at the LGM and contribution of global mean sea level change during the deglaciation. Some of these results are shown in the supporting information (Figures S3–S5).

3. Results

3.1. Northern Hemisphere Ice Volume Changes Over the Last Glacial Cycle

Figure 1 shows NHIS volume variations during the last glacial cycle in simulations performed with the coupled ice sheet-GIA model. In all of the simulations, the NHIS show multiple growth (marked in white bars in Figure 1) and retreat (marked in light yellow bars in Figure 1) phases across the glacial cycle, driven primarily by changes in solar insolation due to cyclical changes in Earth's orbit (i.e., Milankovitch cycles). The initial growth phase starts at ∼120 ka, reaching the first glacial peak at ∼110 ka. Other growth phases occur at 100-90, 77-63 ka and a more gradual buildup into the LGM occurs from 52 to 20 ka. Retreat phases occur at 110-100, 90-77, 63-52, and 20-6 ka (the last deglaciation). We also provide snapshots of ice thickness at various times during the last glacial cycle in Figure S2 to put our results into context with several published reconstructed ice histories (Lambeck et al., 2014; Peltier et al., 2004; Tarasov et al., 2012).

Figures 2a and 2b show ice volume and the rate of change of volume, respectively, in North America, Eurasia and Greenland based on the fully coupled simulation (blue line in Figure 1; Figures 2c and 2d are based on the rigid-IOG simulation shown by the black line in Figure 1). While the volume of the NAISC in our simulations is always greater than that of the EISC (Figures 2a and 2c), the ice loss during retreat phases is not always dominated by the NAISC. The EISC is the dominant contributor to the global mean sea level changes during the first (110-100 ka) and the third (63-52 ka) retreat phases, while the NAISC is the dominant contributor during the second (90-77 ka) and the final (20-6 ka; the last deglaciation) retreat phases. Thus, our results suggest that the evolution of the NHIS over the last glacial cycle is complex and dynamic, and the EISC and the NAISC behave differently at each growth and retreat phase.

3.2. Deformational Effects During Growth and Retreat Phases

In this section, we explore the impact of solid Earth deformation on NHIS evolution by comparing the fully coupled simulation (blue line in Figure 1; Figures 2a and 2b) to the rigid Earth-IOG simulation (black line in Figure 1; Figures 2c and 2d).

A comparison of the blue and red lines with the black line in Figure 1 suggests that incorporating solid Earth deformation leads to larger variations in NHIS volume throughout the last glacial cycle. For example, from ∼77-63 ka, the increase in the volume of the NHIS is ∼40% greater for the deformable Earth case than for the rigid case, and the decrease in ice volume is ∼25% greater during the last deglaciation. In particular, on a rigid Earth, the changes in volume of the NAISC are smaller in magnitude (Figure 2c) and with less variable rates of change (Figure 2d) compared to the deformable Earth case (Figures 2a and 2b). The differences are most pronounced during the retreat phases between 90-77 and 20-6 ka (the last deglaciation). These results indicate that the modeled fluctuations in volume of the NAISC are more sensitive to solid Earth deformation than those of the EISC. The NAISC is larger and thicker than the EISC (e.g., see Figure 3), leading to bedrock deformation that is both greater and more sensitive to deeper, higher viscous structure within the Earth's mantle. The solid Earth therefore takes longer to relax toward isostatic equilibrium following NAISC changes than following EISC changes, and the effects of the deformation on ice surface-elevation

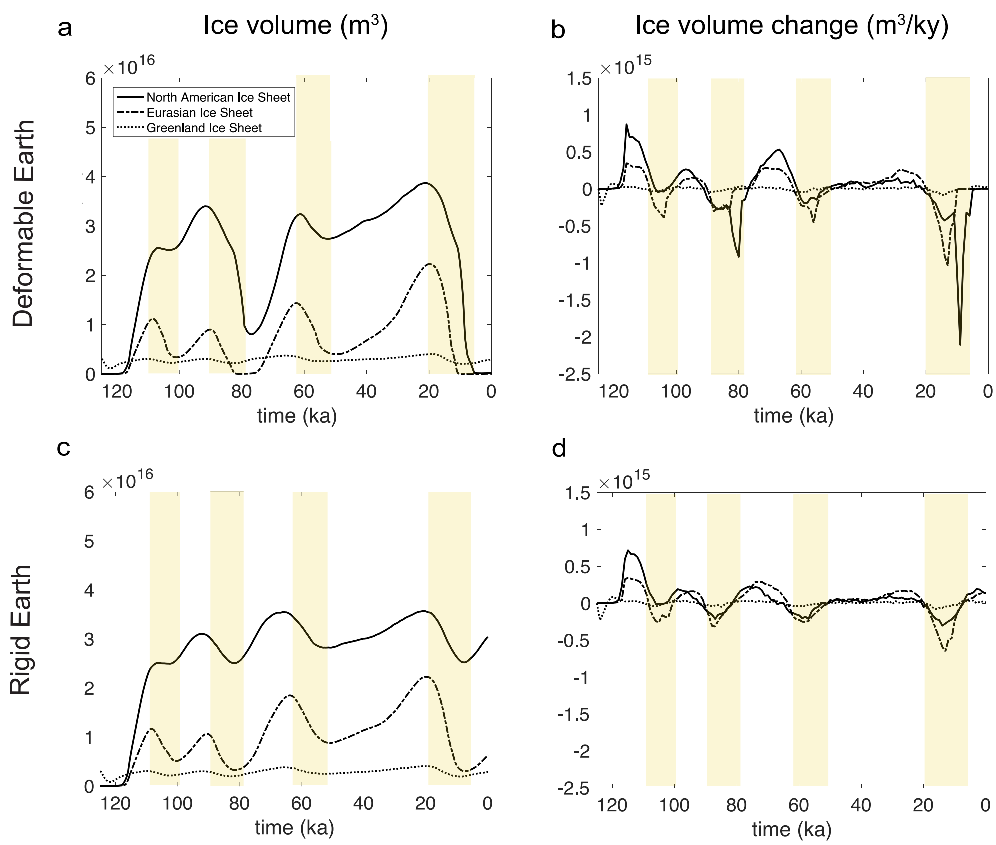

Figure 2. Changes in volume of individual ice sheets on the Northern Hemisphere over the last glacial cycle. (a) Time series of the volume of the North American Ice Sheet Complex (NAISC, solid line), Eurasian Ice Sheet Complex (EISC, dash-dotted line), and the Greenland Ice Sheet (GIS, dotted line) based on the fully coupled simulation (i.e., blue solid line in Figure 1). (b) Rate of change of volume of each ice sheet complex, in units of m^3/ky, calculated based on frame (a). (c and d) Equivalent to frames (a), (b) but calculated from a simulation on a rigid Earth (rigid-IOG simulation, black line in Figure 1).

are enhanced. We also note that the two ice sheet complexes are underlain by different topographic features, which could also pre-dispose the NAISC to be more sensitive to solid earth deformation than the EISC.

Figure 3 explores the impact of solid Earth deformation on changes in the distribution of ice over the Northern Hemisphere during the initial ice growth phase from 120 to 110 ka. During this phase, the LIS in North America advances to cover Hudson Bay (Figures 3a and 3b) with a maximum thickness of ∼3,080 m to the south of the bay (yellow star in Figure 3b). The red line in Figure 3a shows the location of the cross section displayed in Figure 3c. Along this cross section, the LIS reaches a thickness of ∼2,930 m to the south of James Bay at latitude ∼56-degrees North (Figure 3c). The bedrock underneath the ice sheet subsides by up to 315 m from its initial elevation of 200 m below sea level and changes its slope as the ice sheet builds up, lowering the highest point of the ice surface on the cross section down to ∼2,615 m at 110 ka (Figure 3c). When the bedrock elevation is fixed in the rigid Earth-IOG simulation (dashed magenta line in Figure 3c), the ice sheet along the cross section at the same location builds up to a smaller thickness of ∼2,760 m by 110 ka. Since the bedrock elevation at this location remains at 200 m below sea level throughout the 10-ky period, the ice-surface elevation remains at ∼2,960 m, which is ∼245 m higher than on deformable Earth (compare the solid magenta line to the lightest purple line in Figure 3c). In the deformable Earth case, the ice surface remains lower in elevation, and hence, warmer in temperature with higher precipitation relative to the rigid Earth case, allowing the ice sheet to grow thicker (Figure 3d). Note that both simulations begin from the same initial condition, and Figure 3 focuses on the effect of solid Earth deformation during the first growth phase as bedrock elevation between the two simulations initially diverges. Later in the simulations, bedrock elevation differences, and hence, deformational effects on ice cover, are larger (see Figure 1).

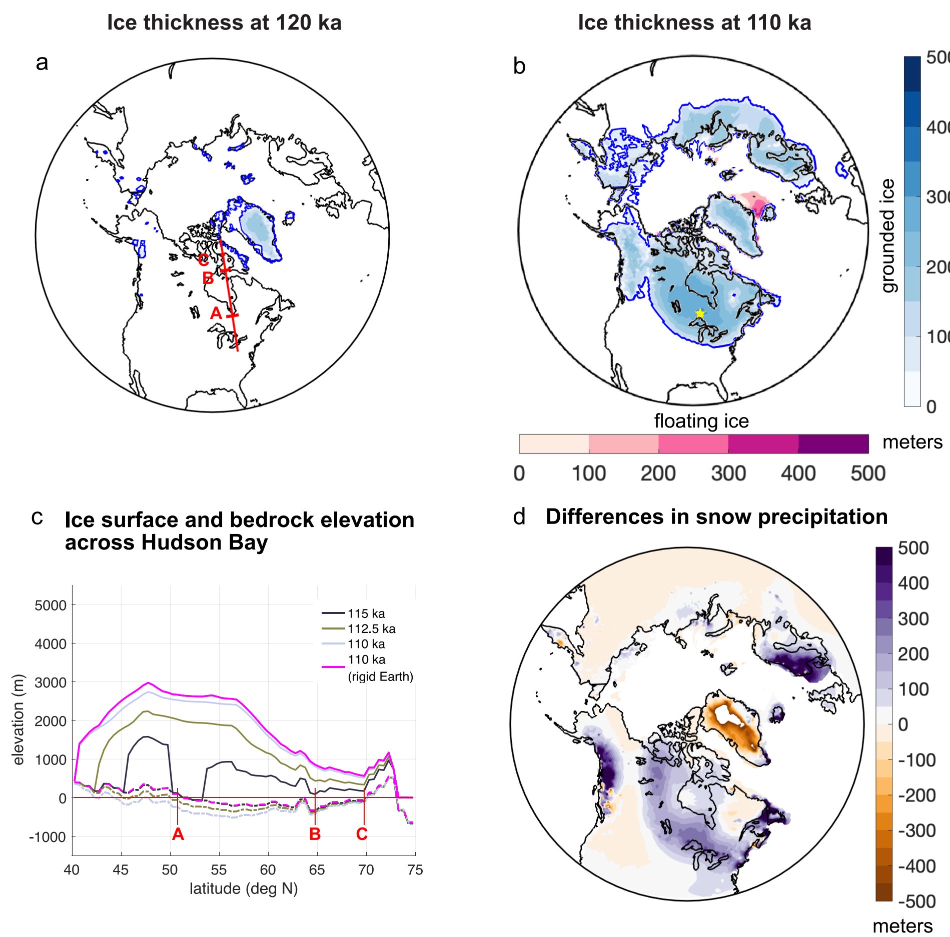

Figure 3. Initial buildup of ice sheet over the Northern Hemisphere between 120 and 110 ka. (a and b) Snapshot of the NHIS at (a) 120 and (b) 110 ka predicted in the fully coupled simulation. Grounded ice and floating ice are represented in blue and magenta, respectively. Blue contour lines show ice sheet grounding lines and black contour lines represent present-day coast lines. The yellow star in frame (b) shows the location where the NHIS reach a maximum thickness 110 ka. (c) Cross section of the elevation of the Laurentide Ice Sheet surface (solid lines) and the bedrock beneath the ice sheet (dashed lines) along Hudson Bay (red line in frame a) at the indicated times between 120 and 110 ka. Magenta lines correspond to the elevation of LIS surface (solid line) and bedrock (dashed line) at 110 ka simulated on the rigid Earth (red line in Figure 1). (d) Difference (deformable minus rigid) in cumulative snowfall over continents, in meters, between the deformable and rigid Earth simulations from 120 to 100 ka.

Next, we explore the impact of solid Earth deformation on an ice cover retreat. Figure 4 focuses on the retreat phase from ~90 to 77 ka, during which differences between the rigid Earth and deformable Earth simulations are the largest (compare the black and blue lines in Figure 1). Similar to the first growth phase shown in Figure 3, the LIS builds up thicker on the deformable Earth than on the rigid Earth during the second growth phase from 100 to 90 ka. Across Hudson Bay by 90 ka on the deformable Earth, the LIS builds up to ~680 m thicker than on the rigid Earth near latitude ~63-degrees North. The highest points of ice-sheet surface are at near latitude ~52-degrees North in both cases, but the ice-surface elevation is ~535 m lower and ice thickness is 295 m greater on the deformable Earth than on the rigid Earth (compare the darkest blue and the magenta lines in Figure 4c). This lower ice-surface elevation on a deformable Earth translates to ~2.35-degree Celsius warmer surface air temperature relative to the rigid Earth case. Additionally, the slope of the bedrock at the edges of the ice sheet becomes more retrograde as the ice sheet advances on the deformable Earth. The resulting increase in surface ablation and the steeper bedrock slope in the deformable Earth case allows the edge of the ice sheet to retreat to Hudson Bay where the retreat accelerates (see the rapid grounding line retreat over the bay from 82.5 to 77.5 ka in Figure 4c). This accelerated retreat is due to both the steeper bedrock slope on the edge of the ice sheet and a slippery marine bed allowing for faster

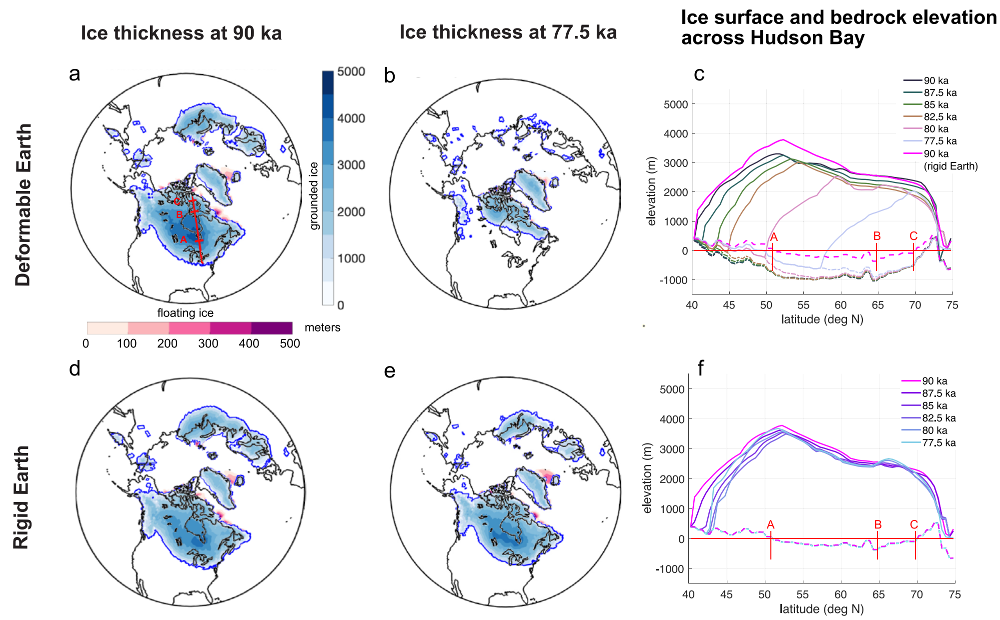

Figure 4. NHIS evolution during the 90-77 ka retreat phase. Snapshots of ice thickness at (a) 90 and (b) 77.5 ka. (c) Cross section of the surface elevation of the Laurentide Ice Sheet (solid lines) and bedrock elevation (dashed lines) along Hudson Bay (red line in frame a) at times between 90 and 77 ka modeled in the fully coupled simulation (solid blue line in Figure 1a). Solid and dashed magenta lines represent the elevation of ice surface end bedrock at 90 ka, respectively, on a rigid Earth. Frames (d–f) are analogous to frames (a–c) but simulated on a rigid Earth.

flow over Hudson Bay (see Section 2). Conversely, on the rigid Earth, the bedrock slope remains unchanged and not enough retreat occurs to reach the unstable region, and Hudson Bay remains ice covered in North America (see Figures 4d–4f).

Overall, Figures 3 and 4 indicate that deformation of the solid Earth enhances thickening (thinning) of ice sheets during growth (retreat) phases in our model. During growth phases, our results show more snow precipitation over a large portion of the area in which ice sheets buildup on the deformable Earth compared to the rigid Earth case (Figure 3d). Lowered ice-surface elevation and warmer air temperature due to solid Earth subsidence allows increased precipitation, which dominates over increased surface melting. During retreat phases, lowered ice surface and delayed uplift of the solid Earth keeps the ice surface lower in elevation, and surface melting dominates over increased precipitation. This positive feedback in both cases leads to greater-magnitude ice volume fluctuations on the deformable Earth than on the rigid Earth in our simulations (i.e., more ice buildup during growth phases between 77-63 and 52-20 ka and more ice loss during retreat phases between 90-77 and 20-6 ka, Figure 1). In the supporting information, we show that our conclusions on the role of deformation on the NHIS evolution remain true in additional fully coupled simulations with varying surface mass balance parameters (Figure S5).

3.3. Gravitational Effects on Marine-Based Ice Sheets During Retreat Phases

The results above show that solid Earth deformation has a positive feedback on ice buildup and retreat over longer timescales ($\geq O10^3$ yr). Next, we focus on the negative feedback of gravitational field perturbations on the evolution of marine sectors of ice in North America and Eurasia on shorter timescales ($\leq O10^2$ yr). Figure 5 illustrates the evolution of the LIS during its rapid retreat between 80 and 78.5 ka over Hudson Bay. Figure 5a shows that until 80 ka, Hudson Bay is covered by the LIS both in the fully coupled simulation and the deformable Earth-noIOG simulation with similar extent (see the grounding lines in blue and red lines). By 79 ka (Figure 5b), the LIS in both simulations undergo marine-based retreat over the bay (i.e., the bedrock elevation at the edge of the ice sheet is negative during the retreat, and hence the ice is marine-terminating). Then, between 79 and 78.5 ka, the ice sheet re-advances into the bay in the fully coupled simulation in which ice-ocean gravity is included. In contrast, the ice sheet continues to retreat when ice-ocean gravity

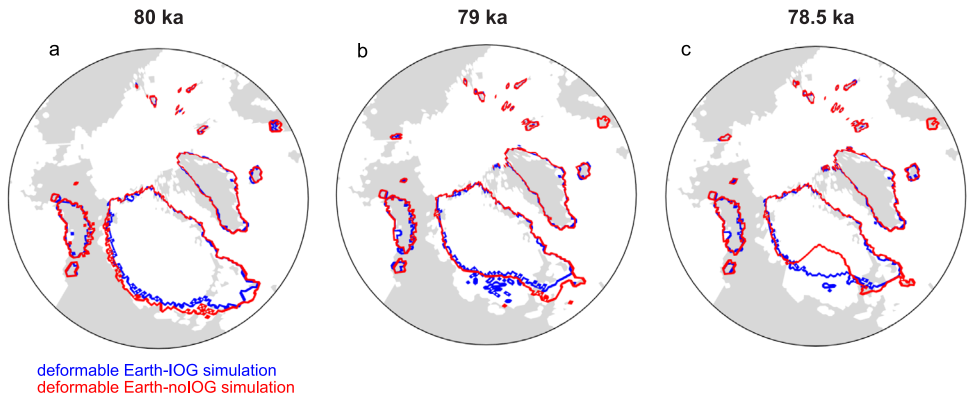

Figure 5. The effect of ice ocean gravity on the extent and timing of retreat over Hudson Bay toward the end of 90-80 ka deglacial phase. At (a) 80 ka, (b) 79 ka, and (c) 78.5 ka. Blue and red lines represent the results from the coupled simulation on a deformable Earth in which ice-ocean gravity is incorporated (i.e., fully coupled simulation) and excluded (i.e., deformable Earth-noIOG coupled simulation), respectively. Positive bedrock topography at respective times are in gray.

is excluded (Figure 5c). When ice-ocean gravity is incorporated, the sea surface height near the retreating ice sheet drops, increasing the sea level fall at the grounding line associated with ice loss. This stronger sea level fall when ice-ocean gravity is incorporated feeds back onto less ice flux across the grounding lines, eventually allowing the grounding lines to re-advance over Hudson Bay.

The Barents-BKIS was a marine-based ice sheet that extended into the Barents and Kara seas north of Siberia and Scandinavia at the LGM. Figure 6 focuses on the impact of ice-ocean gravity on the extent and thickness of the BKIS during the last deglaciation by comparing the fully coupled and deformable Earth-noIOG simulations. In general, the largest differences occur in regions of ice-ocean interface where the ice is marine-terminating and the sea-level feedback on ice dynamics is active. Up until 13 ka, before major retreat in this region, the extent of the BKIS in the two simulations is similar, and differences in ice thickness along the grounding line are less than 100 m (Figure 6a). Between 12.3 ka and 11.5 ka (Figures 6b–6d), the ice sheet retreat is delayed, and ice remains thicker in the fully coupled simulation, which includes ice-ocean gravity. For example, differences in ice thickness reach up to ∼1,260 m in the Kara Sea at 11.8 ka (see the regions in dark yellow in Figure 6c), and at the same time, the grounding line in the deformable Earth-noIOG simulation is up to ∼300 km further inland (Figure 6c). By 11 ka, the two simulations show the similar extent of grounding lines between the two simulations with and without ice-ocean gravity (there is some floating ice remaining in the Barents Sea in the fully coupled simulation; see the yellow region outside of the grounding lines in Figure 6e). The retreat of the BKIS is complete in both simulations by 10.5 ka (Figure 6f). We note that the grounding line differences are relatively small for the NAISC, because not much of the NAISC margin was marine-retreating before 11 ka. Thus, Figures 5 and 6 suggest that the sea-level feedback impacts the timing of marine-based ice sheet retreat during the last deglaciation in the Northern Hemisphere, leading to slowed retreat or re-advance of the ice margin, but does not play a big role in the evolution of ice sheet interiors.

4. Sensitivity of Ice Volume Variations to Adopted Earth and Climate Model Parameters

Our results add to a body of literature showing that the modeled influence of Earth deformation on ice sheet evolution is sensitive to the parameters governing both the sensitivity of the ice sheet model to the timing and magnitude of deformation in the Earth model and to climate. Previous studies have suggested the important role of solid Earth deformation in generating the ∼100-ky periodicity saw-tooth pattern of the Late Quaternary glacial cycles (e.g., Abe-Ouchi et al., 2013; Oerlemans, 1981) and debated the influence of solid Earth deformation during ice growth and retreat phases in the Northern Hemisphere (e.g., Crucifix et al., 2001; van den Berg et al., 2008). Incorporating a simple "Local Lithosphere Relaxing Asthenosphere" (LLRA; see Le Meur & Huybrechts, 1996) bedrock model in a 200 ky-long simulation, Crucifix et al. (2001)

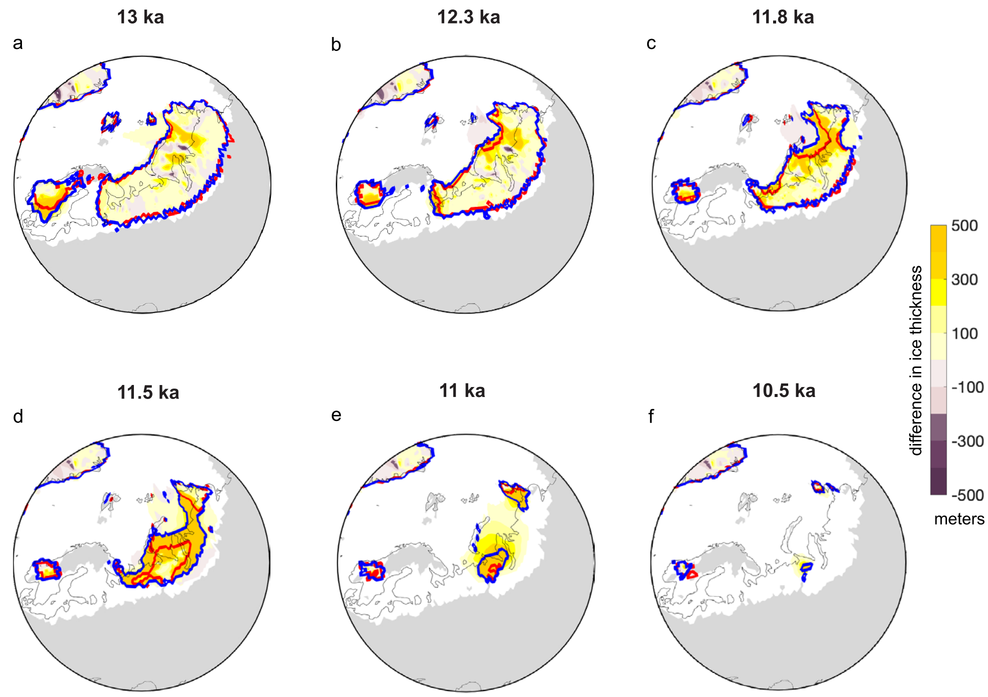

Figure 6. Stabilization of marine-terminating Barents-Kara Ice Sheets due to gravitational effects between 13 and 11 ka during the last deglaciation. (a–f) Differences in ice thickness (in meters) modeled in the coupled simulation in which ice-ocean gravity is incorporated and not incorporated (i.e., fully coupled minus deformable Earth-noIOG) at (a) 13 ka, (b) 12.3 ka, (c) 11.8 ka, (d) 11.5 ka, (e) 11 ka, and (f) 10.5 ka. Blue and red contour lines represent grounding lines of ice sheets in the fully coupled and deformable Earth-noIOG coupled simulations, respectively. Thin black contour lines represent present-day shorelines. Bedrock topography above sea level at respective times are in gray. Note that the color is saturated in frame (c) and (d).

suggested that solid Earth deformation always acts to inhibit ice buildup during growth phases and to enhance ice loss during retreat phases. They also performed sensitivity tests varying bedrock density and relaxation time parameters and showed that their modeled ice volume changes are mainly controlled by the bedrock density parameter in the LLRA model. This parameter influences the equilibrium depression of the bedrock under loading (e.g., a smaller value of bedrock density results in a higher value of equilibrium depression). Their simulations showed that a smaller (higher) value of bedrock density leads to a smaller (higher) ice volume. Later, van den Berg et al. (2008) performed 1-D ice sheet model simulations using an Elastic Lithosphere and Relaxed Asthenosphere (ELRA; see Le Meur & Huybrechts, 1996) bedrock model that incorporates elastic flexure of the lithosphere as well as isostatic relaxation of the asthenosphere and a surface ice mass balance model that better captures the ice-elevation feedback at ice sheet margins. They showed that solid Earth deformation can feed back either positively or negatively on ice buildup depending on the choice of flexural rigidity, which controls the bending of the lithosphere in the bedrock model. They also performed 3-D ice sheet model simulations over Eurasia and showed that a lower value of the flexural rigidity (i.e., more bending of the lithosphere, resulting in more depression under loading and a higher peripheral bulge at the edge of the loading) results in a larger ice sheet.

Unlike the studies mentioned above, our results indicate that solid Earth deformation feeds back positively on ice volume changes, enhancing both ice sheet buildup and retreat (Figures 1–4). In this study, we incorporate a self-gravitating, viscoelastic, spherical Earth model (SGVE) that takes a systematically different and more sophisticated approach to treating isostatic deformation. Previous studies have shown that the largest differences between ELRA and SGVE Earth models occur in the peripheral regions of an ice sheet (e.g., Konrad et al., 2014; Le Meur & Huybrecht, 1996; van den Berg et al., 2008), and the differences also depend on the size of the loading. To test sensitivity of the NHIS dynamics and the effects of solid Earth deformation on NHIS dynamics to varying Earth Structure and surface mass balance parameters, we show the results of additional coupled simulations adopting a range of Earth structure profiles (i.e., lithospheric thickness, upper, and lower mantle viscosities) in the SGVE model (Figure S3) and the surface mass balance parameters in the ice sheet model in the supporting information (Figures S4 and S5). Figure S3 indicates that the NHIS volume is not very sensitive to any single parameter but is more sensitive to a combination of parameters. Simulations with an Earth model that combines a thinner lithosphere and lower mantle viscosities produce larger variations in ice volume than those adopting a thicker lithosphere and higher mantle viscosities. We find that ice volume changes are even more sensitive to the choice of lapse rate and temperature correction (surface mass balance) parameters determining the climate forcing (Figure S4). In particular, we find that both the modeled NHIS volume changes and the sensitivity of the ice volume to solid Earth deformation vary with these parameters (Figure S5); the latter sensitivity increases with the adopted lapse rate. However, we highlight that our main conclusion on the role of deformational effects on NHIS dynamics still holds for the range of surface mass balance parameters and Earth model parameters we explored: Solid Earth deformation acts to enhance ice buildup during growth phases and enhance ice loss during retreat phases. In the context of existing literature, our results suggest that the role of solid Earth deformation on modeled ice sheets depends on both the adopted Earth model (e.g., LLRA, ELRA, or SGVE, with the latter being most realistic; Le Meur & Huybrecht, 1996) and their parameters, and on the surface mass balance model incorporated in the ice sheet model.

5. Discussion and Conclusions

In this study, we coupled a dynamic ice sheet model with a GIA model and applied the coupled model to the Northern Hemisphere over the last glacial cycle. We simulated glaciologically consistent ice sheet dynamics, gravitationally self-consistent sea level change and solid Earth deformation, and explored the feedbacks that arise between these systems. Our results demonstrate that solid Earth deformation enhances buildup during growth phases and melting during retreat phases, leading to more dynamic ice cover changes throughout the last glacial cycle (Figures 1–4). Gravitational effects have a stabilizing influence on marine sectors of ice sheets in both North America and Eurasia during more rapid ($\leq O10^2$ yr) retreat phases (Figures 5 and 6).

Our results suggest that the dynamics and sensitivity to climate of each ice sheet complex in the Northern Hemisphere differed due to deformational effects (Figures 1 and 2). In particular, we find that solid Earth deformation enhances the sensitivity of the NAISC to climate more than the EISC (Figure 2). These findings are in agreement with Bonelli et al. (2009), who simulated the NHIS over the last glacial cycle using a fully coupled climate-ice sheet model and showed that the Laureantide and Fennoscandian Ice Sheet have different responses to atmospheric CO2 concentration and insolation. Adding to their results, we find that the different responses of the EISC and the NAISC to climate may also be associated with differences in solid Earth deformation in response to different sizes of surface loading changes. The dependence of solid Earth deformation on the size of the load has been well explored in other studies (e.g., Crucifix et al., 2001; Le Meur & Huybrechts, 1996; Peltier, 1974; van den Berg et al., 2008).

In addition to being sensitive to the details of the bedrock and climate forcing models (see Figures S3–S5 and discussion in Section 4), our results comparing simulations that include and exclude solid Earth deformation suggest that the magnitude of ice volume variations is sensitive to the initial bedrock condition at the start of every growth and retreat phase. Thus, ice volume changes during the earlier part of the last glacial cycle in our simulations may also depend on the initial bedrock elevation in the last interglacial. The solid Earth was not at isostatic equilibrium at the start of the last glacial cycle, since the glacial maximum of the penultimate glacial cycle (192-135 ka) was only established around 150-140 ka (Colleoni et al., 2016; Grant et al., 2014; Jakobsson et al., 2016; Rohling et al., 2014), and sea level records and modeling indicate ongoing GIA effects throughout the last interglacial (e.g., Clark et al., 2020; Dendy et al., 2017). This ongoing GIA could have influenced initial buildup of the NHIS at the start of the last glacial cycle. In subsequence work, we will apply the coupled model over multiple glacial cycles. The dependence of the rate and magnitude of ice cover changes on initial bedrock state may also provide insight into a possible setting for a rapid glaciation of the LIS from a small-sized configuration during the Marine Isotope Stage 3 to the LGM extent suggested by recent studies on the LIS configuration (e.g., Batchelor et al., 2019; Carlson et al., 2018; Dalton et al., 2019; Pico et al., 2017).

While deformational effects have a strong influence on ice volume variations over continental regions, gravitational effects due to ice-ocean gravity impact the timing and extent of ice sheet retreat regionally in marine terminating areas. For example, we found that the gravitationally driven draw-down of the sea surface due to local ice loss caused marine-ice sheet grounding lines to re-advance or to be delayed in retreat over Hudson Bay and Barents-Kara Seas near the end of the retreat phases (Figures 5 and 6). Existing work has applied coupled ice sheet-sea level modeling to show the stabilizing influence of gravitational effects on marine-sectors of the Antarctic Ice Sheet (deBoer et al., 2014; Gomez et al., 2013, 2015; Konrad et al., 2015). This study suggests that coupled models, which more precisely capture ice sheet-sea level feedbacks in marine areas than models that do not take into account ice-ocean gravity and complex solid Earth deformation, can potentially provide insight into the mechanisms driving marine-based ice sheet dynamics not only in Antarctica but also in Eurasia and North America. For example, these effects may have played a role in the suggested rapid collapse of marine-sectors of the EISC that contributed to the Meltwater Pulse 1A event (Brendryen et al., 2020), in ice stream surging (Andreassen et al., 2014; Bjarnadóttir et al., 2014) and ice-rafted debris fluxes from the EISC during Heinrich Stadial 1 (e.g., Ng et al., 2018; Toucanne et al., 2015), and in the suggested Hudson Bay ice saddle collapse that might explain the 8.2 ka cold event (Gregoire et al., 2012; Lochte et al., 2019; Matero et al., 2017). Furthermore, studying the observed rapid collapse of paleo marine-terminating ice sheets such as the BKIS may, in turn, provide insight into the conditions, mechanisms, timing and extent of future collapse of marine sectors of the Antarctic Ice Sheet, which are a significant source of uncertainty in future sea-level projections (Church et al., 2013).

Data Availability Statement

Data used to generate results are available at http://osf.io/ewpqz.

Acknowledgments
We thank Niall Gandy and other anonymous reviewers for their constructive comments that helped to improve our manuscript. H. K. Han and N. Gomez were supported by Natural Sciences and Engineering Research Council of Canada (NSERC) Discovery Grant, Canada Research Chairs in Ice Sheet—Sea Level Interactions and Canadian Foundation for Innovation. H. K. Han was also funded by McGill Space Institute. R. DeConto was supported by the National Science Foundation (NSF) Office of Polar Programs (OPP) grant OPP-1934477.

References

Abe-Ouchi, A., Saito, F., Kawamura, K., Raymo, M. E., Okuno, J., Takahashi, K., & Blatter, H. (2013). Insolation-driven 100,000-year glacial cycles and hysteresis of ice-sheet volume. *Nature*, *500*, 190–193. https://doi.org/10.1038/nature12374

Abe-Ouchi, A., Segawa, T., & Saito, F. (2007). Climatic conditions for modelling the Northern Hemisphere ice sheets throughout the ice age cycle. *Climate of the Past*, *3*, 423–438. https://doi.org/10.5194/cp-3-423-2007

Andreassen, K., Winsborrow, M. C. M., Bjarnadóttir, L. R., & Rüther, D. C. (2014). Ice stream retreat dynamics inferred from an assemblage of landforms in the northern Barents Sea. *Quaternary Science Reviews*, *92*, 246–257. https://doi.org/10.1016/j.quascirev.2013.09.015

Argus, D. F., Peltier, W. R., Drummond, R., & Moore, A. W. (2014). The Antarctica component of postglacial rebound model ICE-6G_C (VM5a) based on GPS positioning, exposure age dating of ice thicknesses, and relative sea level histories. *Geophysical Journal International*, *198*, 537–563. https://doi.org/10.1093/gji/ggu140

Austermann, J., Mitrovica, J. X., Latychev, K., & Milne, G. A. (2013). Barbados-based estimate of ice volume at Last Glacial Maximum affected by subducted plate. *Nature Geoscience*, *6*, 553–557. https://doi.org/10.1038/ngeo1859

Banderas, R., Alvarez-Solas, J., Robinson, A., & Montoya, M. (2018). A new approach for simulating the paleo-evolution of the Northern Hemisphere ice sheets. *Geoscientific Model Development*, *11*, 2299–2314. https://doi.org/10.5194/gmd-11-2299-2018

Bassis, J. N., Petersen, S. V., & Mac Cathles, L. (2017). Heinrich events triggered by ocean forcing and modulated by isostatic adjustment. *Nature*, *542*, 332–334. https://doi.org/10.1038/nature21069

Batchelor, C. L., Margold, M., Krapp, M., Murton, D. K., Dalton, A. S., Gibbard, P. L., et al. (2019). The configuration of Northern Hemisphere ice sheets through the Quaternary. *Nature Communications*, *10*, 3713. https://doi.org/10.1038/s41467-019-11601-2

Beghin, P., Charbit, S., Dumas, C., Kageyama, M., Roche, D. M., & Ritz, C. (2014). Interdependence of the growth of the Northern Hemisphere ice sheets during the last glaciation: The role of atmospheric circulation. *Climate of the Past*, *10*, 345–358. https://doi.org/10.5194/cpd-9-2183-2013

Berends, C. J., de Boer, B., & van de Wal, R. S. W. (2018). Application of HadCM3@Bristolv1.0 simulations of paleoclimate as forcing for an ice-sheet model, ANICE2.1: Set-up and benchmark experiments. *Geoscientific Model Development*, *11*, 4657–4675. https://doi.org/10.5194/gmd-11-4657-2018

Bjarnadóttir, L. R., Winsborrow, M. C. M., & Andreassen, K. (2014). Deglaciation of the central Barents Sea. *Quaternary Science Reviews*, *92*, 208–226. https://doi.org/10.1016/j.quascirev.2013.09.012

Bonelli, S., Charbit, S., Kageyama, M., Woillez, M. -N., Ramstein, G., Dumas, C., & Quiquet, A. (2009). Investigating the evolution of major Northern Hemisphere ice sheets during the last glacial-interglacial cycle. *Climate of the Past*, *5*, 329–345. https://doi.org/10.5194/cpd-5-1013-2009

Brendryen, J., Haflidason, H., Yokoyama, Y., Haaga, K. A., & Hannisdal, B. (2020). Eurasian Ice Sheet collapse was a major source of Meltwater Pulse 1A 14,600 years ago. *Nature Geoscience, 13*, 1–6. https://doi.org/10.1038/s41561-020-0567-4

Carlson, A. E., Tarasov, L., & Pico, T. (2018). Rapid Laurentide ice-sheet advance toward southern last glacial maximum limit during Marine Isotope Stage 3. *Quaternary Science Reviews*, *196*, 118–123. https://doi.org/10.1016/j.quascirev.2018.07.039

Charbit, S., Dumas, C., Kageyama, M., Roche, D. M., & Ritz, C. (2013). Influence of ablation-related processes in the build-up of simulated Northern Hemisphere ice sheets during the last glacial cycle. *The Cryosphere*, *7*, 681–698. https://doi.org/10.5194/tc-7-681-2013

Charbit, S., Ritz, C., Philippon, G., Peyaud, V., & Kageyama, M. (2007). Numerical reconstructions of the Northern Hemisphere ice sheets through the last glacial-interglacial cycle. *Climate of the Past*, *3*, 15–37. https://doi.org/10.5194/cp-3-15-2007

Church, J. A., Clark, P. U., Cazenave, A., Gregory, J. M., Jevrejeva, S., Levermann, A., et al. (2013). Sea level change. In T. F. Stocker, D. Qin, G.-K. Plattner, M. Tignor, S. K. Allen, J. Boschung, et al. (Eds.), *Climate Change 2013: The physical science basis. Contribution of Working Group I to the Fifth Assessment Report of the Intergovernmental Panel on Climate Change*. Cambridge, UK and New York, NY: Cambridge University Press.

Clark, P. U., Dyke, A. S., Shakun, J. D., Carlson, A. E., Clark, J., Wohlfarth, B., et al. (2009). The Last Glacial Maximum. *Science*, *325*, 710–714. https://doi.org/10.1126/science.1172873

Clark, P. U., He, F., Golledge, N. R., Mitrovica, J. X., Dutton, A., Hoffman, J. F., & Dendy, S. (2020). Oceanic forcing of penultimate deglacial and last interglacial sea-level rise. *Nature*, *577*, 660–664. https://doi.org/10.1038/s41586-020-1931-7

Colleoni, F., Wekerle, C., Näslund, J. -O., Brandefelt, J., & Masina, S. (2016). Constraint on the penultimate glacial maximum Northern Hemisphere ice topography (∼ 140 kyrs BP). *Quaternary Science Reviews*, *137*, 97–112. https://doi.org/10.1016/j.quascirev.2016.01.024

Crucifix, M., Loutre, M. -F., Lambeck, K., & Berger, A. (2001). Effect of isostatic rebound on modelled ice volume variations during the last 200 kyr. *Earth and Planetary Science Letters*, *184*, 623–633. https://doi.org/10.1016/S0012-821X(00)00361-7

Cuzzone, J. K., Clark, P. U., Carlson, A., Ullman, D., Rinterknecht, R., Milne, G. A., et al. (2016). Final deglaciation of the Scandinavian Ice Sheet and implications for the Holocene global sea-level budget. *Earth and Planetary Science Letters*, *448*, 34–41. https://doi.org/10.1016/j.epsl.2016.05.019

Dalton, A. S., Finkelstein, S. A., Forman, S. L., Barnett, P. J., Pico, T., & Mitrovica, J. X. (2019). Was the Laurentide Ice Sheet significantly reduced during Marine Isotope Stage 3? *Geology*, *47*, 111–114. https://doi.org/10.1130/G45335.1

de Boer, B., Stocchi, P., & van de Wal, R. S. W. (2014). A fully coupled 3-D ice-sheet–sea-level model: Algorithm and applications. *Geoscientific Model Development*, *7*, 2141–2156. https://doi.org/10.5194/gmd-7-2141-2014

DeConto, R. M., & Pollard, D. (2003). Rapid Cenozoic glaciation of Antarctica induced by declining atmospheric CO_2. *Nature*, *421*(6920), 245–249. http://doi.org/10.1038/nature01290

Dendy, S., Austermann, J., Creveling, J., & Mitrovica, J. X. (2017). Sensitivity of Last Interglacial sea level high stands to ice sheet configuration during Marine Isotope Stage 6 S. *Quaternary Science Reviews*, *171*, 234–244. https://doi.org/10.1016/j.quascirev.2017.06.013

Denton, G. H., & Hughes, T. J. (1981). The last great ice sheets. In *The Arctic ice sheet: An outrageous hypothesis*. New York, NY: Wiley Interscience.

Drouet, A. S., Docquier, D., Durand, G., Hindmarsh, R., Pattyn, F., Gagliardini, O., & Zwinger, T. (2013). Grounding line transient response in marine ice sheet models. *The Cryosphere*, *7*, 395–406. https://doi.org/10.5194/tc-7-395-2013

Dyke, A. S. (2004). An outline of North American deglaciation with emphasis on central and northern Canada. In J. Ehlers & P. L. Gibbard (Eds.), *Quarternary glaciations – extent and chronology, Part II* (pp. 373–424). Amsterdam: Elsevier. https://doi.org/10.1016/S1571-0866(04)80209-4

Dyke, A. S., Andrews, J. T., Clark, P. U., England, J. H., Miler, G. H., Shaw, J., & Veillette, J. J. (2002). The Laurentide and Innuitian ice sheets during the Last Glacial Maximum. *Quaternary Science Reviews*, *21*, 9–31.

Dziewonski, A. M., & Anderson, D. L. (1981). Preliminary reference Earth model. *Physics of the Earth and Planetary Interiors*, *25*, 297–356. http://dx.doi.org/10.1016/0031-9201(81)90046-7

Erokhina, O., Rogozhina, I., Prange, M., & Bakker, P. (2017). Dependence of slope lapse rate over the Greenland ice sheet on background climate. *Journal of Glaciology*, *63*(239), 568–572. https://doi.org/10.1017/jog.2017.10

Fairbanks, R. G. (1989). A 17,000-year glacio-eustatic sea level record: Influence of glacial melting rates on the Younger Dryas event and deep-ocean circulation. *Nature*, *342*, 637–642. https://doi.org/10.1038/342637a0

Farrell, W. E., & Clark, J. A. (1976). On postglacial sea level. *Geophysical Journal of the Royal Astronomical Society*, *46*, 647–667. https://doi.org/10.1111/j.1365-246X.1976.tb01252.x

Fleming, K., & Lambeck, K. (2004). Constraints on the Greenland Ice Sheet since the Last Glacial Maximum from sea-level observations and glacial-rebound models. *Quaternary Science Reviews*, *23*, 1053–1077. https://doi.org/10.1016/j.quascirev.2003.11.001

Ganopolski, A., Calov, R., & Claussen, M. (2010). Simulation of the last glacial cycle with a coupled climate ice-sheet model of intermediate complexity. *Climate of the Past*, *6*, 229–224. https://doi.org/10.5194/cp-6-229-2010

Gomez, N., Latychev, K., & Pollard, D. (2018). A Coupled Ice Sheet–Sea Level Model Incorporating 3D Earth Structure: Variations in Antarctica during the Last Deglacial retreat. *Journal of Climate*, *31*, 4041–4054. https://doi.org/10.1175/JCLI-D-17-0352.1

Gomez, N., Mitrovica, J. X., Huybers, P., & Clark, P. U. (2010). Sea level as a stabilizing factor for marine-ice-sheet grounding lines. *Nature Geoscience*, *3*, 850–853. https://doi.org/10.1038/ngeo1012

Gomez, N., Pollard, D., & Holland, D. (2015). Sea-level feedback lowers projections of future Antarctic Ice-Sheet mass loss. *Nature Communications*, *6*, 8798. https://doi.org/10.1038/ncomms9798

Gomez, N., Pollard, D., & Mitrovica, J. X. (2013). A 3-D coupled ice sheet – Sea level model applied to Antarctica through the last 40 ky. *Earth and Planetary Science Letters*, *384*, 88–99. https://doi.org/10.1016/j.epsl.2013.09.042

Gowan, E., Niu, L., Knorr, G., & Lohmann, G. (2019). Geology datasets in North America, Greenland and surrounding areas for use with ice sheet models. *Earth System Science Data*, *11*, 375–391. https://doi.org/10.5194/essd-11-375-2019

Grant, K. M., Rohling, E. J., Ramsey, C. B., Cheng, H., Edwards, R. L., Florindo, F., et al. (2014). Sea-level variability over five glacial cycles. *Nature Communications*, *5*, 5076. https://doi.org/10.1038/ncomms6076

Gregoire, L. J., Payne, A. J., & Valdes, P. J. (2012). Deglacial rapid sea level rises caused by ice-sheet saddle collapses. *Nature*, *487*, 219–222. https://doi.org/10.1038/nature11257

Gregoire, L. J., Valdes, P. J., & Payne, A. J. (2015). The relative contribution of orbital forcing and greenhouse gases to the North American deglaciation. *Geophysical Research Letters*, *42*, 9970–9979. https://doi.org/10.1002/2015GL066005

Harrison, S., Smith, D. E., & Glasser, N. F. (2019). Late Quaternary meltwater pulses and sea level change. *Journal of Quaternary Science*, *34*, 1–15. https://doi.org/10.1002/jqs.3070

Heinrich, H. (1988). Origin and consequences of cyclic ice rafting in the Northeast Atlantic Ocean during the Past 130,000 years. *Quaternary Research*, *29*(2), 142–152. http://doi.org/10.1016/0033-5894(88)90057-9

Hughes, A. L. C., Gyllencreutz, R., Lohne, Ø. S., Mangerud, J., & Svendsen, J. I. (2016). The last Eurasian ice sheets – A chronological database and time-slice reconstruction, DATED-1. *Boreas*, *45*, 1–45. https://doi.org/10.1111/bor.12142

Jakobsson, M., Nilsson, J., Anderson, L., Backman, J., Bjorkm, G., Cronin, T. M., et al. (2016). Evidence for an ice shelf covering the central Arctic Ocean during the penultimate glaciation. *Nature Communications*, *7*, 10365. https://doi.org/10.1038/ncomms10365

Kendall, R. A., Mitrovica, J. X., & Milne, G. A. (2005). On post-glacial sea level – II. Numerical formulation and comparative results on spherically symmetric models. *Geophysical Journal International*, *161*, 679–706. https://doi.org/10.1111/j.1365-246X.2005.02553.x

Kleman, J., Fastook, J., Ebert, K., Nilsson, J., & Caballero, R. (2013). Pre-LGM Northern Hemisphere ice sheet topography. *Climate of the Past*, *9*, 2365–2378. https://doi.org/10.5194/cp-9-2365-2013

Kleman, J., Jansson, K., De Angelis, H., Stroeven, A. P., Hättestrand, C., Alm, G., & Glasser, N. (2010). North American Ice Sheet build-up during the last glacial cycle, 115-21 kyr. *Quaternary Science Reviews*, *29*, 2036–2051. https://doi.org/10.1016/j.quascirev.2010.04.021
Konrad, H., Sasgen, I., Pollard, D., & Klemann, V. (2015). Potential of the solid-Earth response for limiting long-term West Antarctic Ice Sheet retreat in a warming climate. *Earth and Planetary Science Letters*, *432*, 254–264. https://doi.org/10.1016/j.epsl.2015.10.008
Konrad, H., Thoma, M., Sasgen, I., Klemann, V., Grosfeld, K., Barbi, D., & Martinec, Z. (2014). The deformational response of a viscoelastic Solid Earth model coupled to a thermomechanical ice sheet model. *Surveys in Geophysics*, *35*, 1441–1458. http://doi.org/10.1007/s10712-013-9257-8
Lambeck, K., Rouby, H., Purcell, A., Sun, A., & Sambridge, M. (2014). Sea level and global ice volumes from the Last Glacial Maximum to the Holocene. *Proceedings of the National Academy of Sciences of the United States of America*, *111*, 15296–15303.
Le Meur, E., & Huybrechts, P. (1996). A comparison of different ways of dealing with isostasy: Examples from modelling the Antarctic ice sheet during the last glacial cycle. *Annals of Glaciology*, *23*, 309–317. https://doi.org/10.3189/S0260305500013586
Levermann, A., & Winkelmann, R. (2016). A simple equation for the melt elevation feedback of ice sheets. *The Cryosphere*, *10*, 1799–1807. https://doi.org/10.5194/tc-10-1799-2016
Liakka, J., Lofverstrom, M., & Colleoni, F. (2016). The impact of the North American glacial topography on the evolution of the Eurasian ice sheet over the last glacial cycle. *Climate of the Past*, *12*, 1225–1241. https://doi.org/10.5194/cp-12-1225-2016
Lisiecki, L., & Raymo, M. (2005). A Pliocene-Pleistocene stack of 57 globally distributed benthic $\delta^{18}O$ records. *Paleoceanography*, *20*, PA1003. https://doi.org/10.1029/2004PA001071
Lochte, A. A., Repschläger, J., Kienast, M., Garbe-Schönberg, D., Andersen, N., Hamann, C., & Schneider, R. (2019). Labrador Sea freshening at 8.5 ka BP caused by Hudson Bay Ice Saddle collapse. *Nature Communications*, *10*, 586. https://doi.org/10.1038/s41467-019-08408-6
MacAyeal, D. R. (1993). Binge/purge oscillations of the Laurentide Ice Sheet as a cause of the North Atlantic's Heinrich events. *Paleoceanography*, *8*(6), 775–784. https://doi.org/10.1029/93PA02200
Marshall, S., James, T., & Clarke, G. (2002). North American Ice Sheet reconstruction at the Last Glacial Maximum. *Quaternary Science Reviews*, *21*, 175–192. https://doi.org/10.1016/S0277-3791(01)00089-0
Matero, I. S. O., Gregoire, L. J., Ivanovic, R. F., Tindall, J. C., & Haywood, A. M. (2017). The 8.2 ka cooling event caused by Laurentide ice saddle collapse. *Earth and Planetary Science Letters*, *473*, 205–214. https://doi.org/10.1016/j.epsl.2017.06.011
Mitrovica, J. X., & Milne, G. A. (2002). On the origin of late Holocene sea-level highstands within equatorial ocean basins. *Quaternary Science Reviews*, *21*, 2179–2190. https://doi.org/10.1016/S0277-3791(02)00080-X
Mitrovica, J. X., & Milne, G. A. (2003). On post-glacial sea level: I. General theory. *Geophysical Journal International*, *154*, 253–267. https://doi.org/10.1029/2001GL014273
Mitrovica, J. X., Milne, G. A., & Davis, J. L. (2001). Glacial isostatic adjustment on a rotating Earth. *Geophysical Journal International*, *147*, 562–578. https://doi.org/10.1046/j.1365-246x.2001.01550.x
National Geophysical Data Center. (2006). *2-minute Gridded Global Relief Data (ETOPO2) v2*. NOAA. http://doi.org/10.7289/V5J1012Q
Ng, H. C., Robinson, L. F., McManus, J. F., Mohamed, K. J., Jacobel, A. W., & Ivanovic, R. F. (2018). Coherent deglacial changes in western Atlantic Ocean circulation. *Nature Communications*, *9*, 2947. https://doi.org/10.1038/s41467-018-05312-3
Niu, L., Lohmann, G., Hinck, S., Gowan, E. J., & Krebs-Kanzow, U. (2019). The sensitivity of Northern Hemisphere ice sheets to atmospheric forcing during the last glacial cycle using PMIP3 models. *Journal of Glaciology*, *65*(252), 645–661. https://doi.org/10.1017/jog.2019.42
Oerlemans, J. (1981). Some basic experiments with a vertically-integrated ice sheet model. *Tellus*, *33*(1), 1–11.
Pattyn, F., & Durand, G. (2013). Why marine ice sheet model predictions may diverge in estimating future sea-level rise. *Geophysical Research Letters*, *40*, 4316–4320. https://doi.org/10.1002/grl.50824
Pattyn, F., Perichon, L., Durand, G., Favier, L., Gagliardini, O., Hindmarsh, R. C. A., et al. (2013). Grounding-line migration in plan-view marine ice-sheet models: Results of the ice2sea MISMIP3d intercomparison. *Journal of Glaciology*, *59*, 410–422. https://doi.org/10.3189/2013JoG12J129
Pattyn, F., Schoof, C., Perichon, L., Hindmarsh, R. C. A., Bueler, E., deFleurian, B., et al (2012). Results of the marine ice sheet model intercomparison project, MISMIP. *The Cryosphere*, *6*, 573–588. https://doi.org/10.5194/tc-6-573-2012
Peltier, W. R. (1974). The impulse response of a Maxwell Earth. *Reviews of Geophysics and Space Physics*, *12*(4), 649–669. https://doi.org/10.1029/RG012i004p00649
Peltier, W. R. (2004). The ICE-5G (VM2) Model and GRACE. *Annual Review of Earth and Planetary Sciences*, *32*, 111–149. https://doi.org/10.1146/annurev.earth.32.082503.144359
Peltier, W. R., Argus, D. F., & Drummond, R. (2015). Space geodesy constrains ice age terminal deglaciation: The global ICE-6G_C (VM5a) model. *Journal of Geophysical Research: Solid Earth*, *120*, 450–487. https://doi.org/10.1002/2014JB011176
Pico, T., Creveling, J. R., & Mitrovica, J. X. (2017). Sea-level records from the U.S. mid-Atlantic constrain Laurentide Ice Sheet extent during Marine Isotope Stage 3. *Nature Communications*, *8*, 15612. https://doi.org/10.1038/ncomms15612
Pollard, D. (2010). A retrospective look at coupled ice sheet-climate modeling. *Climate Change*, *100*, 173–194. https://doi.org/10.1007/s10584-010-9830-9
Pollard, D., & DeConto, R. M. (2005). Hysteresis in Cenozoic Antarctic ice-sheet variations. *Global and Planetary Change*, *45*, 9–21. https://doi.org/10.1016/j.gloplacha.2004.09.011
Pollard, D., & DeConto, R. M. (2009). Modeling West Antarctic ice sheet growth and collapse through the past five million years. *Nature*, *458*, 329–332. https://doi.org/10.1038/nature07809
Pollard, D., & DeConto, R. M. (2012). Description of a hybrid ice sheet-shelf model, and application to Antarctica. *Geoscientific Model Development*, *5*, 1273–1295. https://doi.org/10.5194/gmd-5-1273-2012
Rohling, E. J., Foster, G. L., Grant, K. M., Marino, G., Roberts, A. P., Tamisiea, M. E., & Williams, F. (2014). Sea-level and deep-sea-temperature variability over the past 5.3 million years. *Nature*, *508*, 477–482. https://doi.org/10.1038/nature13230
Schoof, C. (2007). Ice sheet grounding line dynamics: Steady states, stability, and hysteresis. *Journal of Geophysical Research*, *112*, F03S28. https://doi.org/10.1029/2006JF000664
Shepherd, A. (2018). Mass balance of the Antarctic Ice Sheet from 1992 to 2017. *Nature*, *558*, 219–222. https://doi.org/10.1038/s41586-018-0179-y
Stokes, C. R., Tarasov, L., & Dyke, A. S. (2012). Dynamics of the North American Ice Sheet Complex during its inception and build-up to the Last Glacial Maximum. *Quaternary Science Reviews*, *50*, 86–104. https://doi.org/10.1016/j.quascirev.2012.07.009
Svendsen, J. I., Alexanderson, H., Astakhov, V. I., Demidov, I., Dowdeswell, J. A., Funder, S., et al. (2004). Late Quaternary ice sheet history of northern Eurasia. *Quaternary Science Reviews*, *23*, 1229–1271. https://doi.org/10.1016/j.quascirev.2003.12.008

Tarasov, L., Dyke, A. S., Neal, R. M., & Peltier, W. R. (2012). A data-calibrated distribution of deglacial chronologies for the North American ice complex from glaciological modeling. *Earth and Planetary Science Letters*, *315–316*, 30–40. https://doi.org/10.1016/j.epsl.2011.09.010

Tarasov, L., & Peltier, W. R. (1997). A high-resolution model of the 100 ka ice-age cycle. *Annals of Glaciology*, *25*, 58–65. https://doi.org/10.1017/S026030550001380X

Thompson, S. L., & Pollard, D. (1997). Greenland and Antarctic mass balances for present and doubled atmospheric CO_2 from the GENESIS Version-2 Global Climate Model. *Journal of Climate*, *10*, 871–900. https://doi.org/10.1175/1520-0442(1997)010<0871:GAAMBF>2.0.CO;2

Timmermann, A., Knies, J., Timm, E., Abe-Ouchi, A., & Friedrich, T. (2010). Promotion of glacial ice sheet buildup 60–115 kyr B.P. by precessionally paced Northern Hemispheric meltwater pulses. *Paleoceanography*, *25*, PA4208. https://doi.org/10.1029/2010PA001933

Toucanne, S., Soulet, G., Freslon, N., Jacinto, R. S., Dennielou, B., Zaragosi, S., et al. (2015). Millennial-scale fluctuations of the European Ice Sheet at the end of the last glacial, and their potential impact on global climate. *Quaternary Science Reviews*, *123*, 113–133. https://doi.org/10.1016/j.quascirev.2015.06.010

Ullman, D. J., Carlson, A. E., Anslow, F. S., LeGrande, A. N., & Licciardi, J. M. (2015). Laurentide ice-sheet instability during the last deglaciation. *Nature Geoscience*, *8*, 534–537. https://doi.org/10.1038/ngeo2463

Ullman, D. J., Carlson, A. E., Hostetler, S. W., Clark, P. U., Cuzzone, J., Milne, G. A., et al. (2016). Final Laurentide ice-sheet deglaciation and Holocene climate-sea level change. *Quaternary Science Reviews*, *152*, 49–59. https://doi.org/10.1016/j.quascirev.2016.09.014

van den Berg, J., van de Wal, R. S. W., Milne, G. A., & Oerlemans, J. (2008). Effect of isostasy on dynamical ice sheet modeling: A case study for Eurasia. *Journal of Geophysical Research*, *113*, B05412. https://doi.org/10.1029/2007JB004994

Weertman, J. (1957). On the sliding of glaciers. *Journal of Glaciology*, *3*(21), 33–38. https://doi.org/10.3189/S0022143000024709

Weertman, J. (1974). Stability of the junction of an ice sheet and an ice shelf. *Journal of Glaciology*, *13*, 3–11.

Yokoyama, Y., Hirabayashi, S., Goto, K., Okuno, J., Sproson, A. D., Haraguchi, T., et al. (2019). Holocene Indian Ocean sea level, Antarctic melting history and past Tsunami deposits inferred using sea level reconstructions from the Sri Lankan, Southeastern Indian and Maldivian coasts. *Quaternary Science Reviews*, *206*, 150–161. https://doi.org/10.1016/j.quascirev.2018.11.024

Zweck, C., & Huybrechts, P. (2005). Modeling of the northern hemisphere ice sheets during the last glacial cycle and glaciological sensitivity. *Journal of Geophysical Research*, *110*, D07103. https://doi.org/10.1029/2004JD005489